EKF for Joint Mitigation of Phase Noise, Frequency Offset and Nonlinearity in 400 Gb/s PM-16-QAM and 200 Gb/s PM-QPSK Systems

Ankita Jain,[1] **Pradeep Kumar Krishnamurthy,**[1] **Pascal Landais,**[2] **and Prince M. Anandarajah**[2]

[1]Center for Lasers and Photonics, Indian Institute of Technology Kanpur, Kanpur 208016, India
[2]School of Electronic Engineering, Dublin City University, Dublin 9, Ireland

1. Introduction

With the growing need for networking, the demand for bandwidth and capacity of data transmission is increasing day-by-day. Looking beyond 100 Gbps, work is already underway towards 400 Gbps data rate as the next ethernet (IEEE 802.3) standard [1]–[3]. For a fixed bandwidth, data rate can be increased by using higher order modulation formats such as 16 and 64 quadrature amplitude

modulation (QAM). While these modulation formats lead to efficient spectrum utilization, they are highly sensitive to frequency offsets, accumulated phase noise and fiber nonlinearities.

Several DSP algorithms have been developed to mitigate these impairments. Viterbi-Viterbi carrier phase estimation (VV-CPE) and its variants are widely used to mitigate frequency offset (FO) and laser phase noise (PN) effects whereas digital backpropagation (DBP) is used to alleviate fiber nonlinearities [4]–[7]. However, DBP can eliminate only deterministic nonlinearities viz. self phase modulation (SPM) and fails to converge to the exact transmitted signal in the presence of nonlinear phase noise (NLPN) induced due to amplified spontaneous emission (ASE) noise interacting with fiber kerr nonlinearity [8]–[10]. Further, VV-CPE algorithm which mainly employs M^{th}-power method is prone to cycle-slipping [11].

The Kalman filtering algorithm is a well-known recursive algorithm for signal estimation and tracking in time-varying systems. At the discrete time step k, the system is specified by a state vector $\mathbf{x_k}$, input vector $\mathbf{u_k}$, and measurement vector $\mathbf{z_k}$. In the Kalman filter (KF) framework, these states are updated according to following equations:

$$\text{Process equation :} \quad \mathbf{x_{k+1}} = \mathbf{f(x_k)} + \mathbf{g(u_k)} + \mathbf{w_k}$$

$$\text{Measurement equation :} \quad \mathbf{z_k} = \mathbf{h(x_k)} + \mathbf{v_k}$$

$$\text{State-update equation :} \quad \mathbf{\hat{x}_{k|k}} = \mathbf{\hat{x}_{k|k-1}} + \mathbf{K_k(z_k - h(\hat{x}_{k|k-1}))}. \tag{1}$$

KF is optimal in the minimum mean square sense for linear systems, i.e., $\mathbf{f(x_k)} = \mathbf{Ax_k}$ with process noise $\mathbf{w_k}$ and measurement noise $\mathbf{v_k}$ as Gaussian and uncorrelated with each other [12], [13]. In optical communication systems, KF has been proposed for estimation and tracking of polarization, phase and frequency offset by treating them as state variables and received samples forming the measurement variables [14], [15]. In [16], KF was used to estimate FO. PN and nonlinearity were not considered. We previously proposed the use of KF in [17] to mitigate PN and NLPN in 100 Gbps single polarization quadrature phase shift keying (QPSK) systems and showed that KF provides 6 dB improvement in Q-factor in comparison with DBP algorithm (1 step/span).

When $\mathbf{f(x_k)}$ is nonlinear, a modified version of KF, suitable for nonlinear dynamic systems, known as extended Kalman filter (EKF) is used [18]. This is desirable in coherent optical communication systems since the received sample r_k is a nonlinear function of phase noise θ_k, i.e. $r_k = s_k e^{j\theta_k} + n_k$. Thus, in EKF r_k can be processed directly without the extraction of phase from r_k as required in KF. In [19], EKF-based carrier phase and amplitude noise estimation (CPANE) algorithm was suggested to jointly mitigate phase and amplitude noise in 224 Gbps coherent optical systems. However, FO was not considered. In real time systems, the frequency offset between transmitter and local oscillator lasers ranges up to few GHz and it is not possible to estimate the phase correctly until FO is compensated [20]. The algorithm in [19] cannot be extended in a straightforward way to include the effects of FO. Thus, a separate algorithm must be used to estimate FO or their algorithm must be reformulated by considering FO as additional state variable. Hence, the computational complexity of EKF is inevitable.

In this paper, we demonstrate the use of extended Kalman filter to simultaneously track and compensate laser PN, FO, and nonlinearity in 400 Gbps polarization multiplexed 16-QAM (PM-16-QAM) and 200 Gbps polarization multiplexed QPSK (PM-QPSK) system. We also compare our results with CPANE. We show that even at high FO of 1 GHz, EKF performs better than CPANE for both PM-16-QAM and PM-QPSK eliminating the requirement of a separate algorithm for mitigating FO.

The remainder of the paper is organised as follows: in Section II, we discuss the system model and DSP techniques used at the receiver end. The extended Kalman filter used for phase and offset estimation is described in Section III. In Section IV, we present simulation results showing the performance of EKF for back-to-back as well as transmission over 10-span link for both 400 Gbps PM-16-QAM and 200 Gbps PM-QPSK. We conclude by summarizing our results in Section V.

2. System Model

In order to access the performance of EKF for the joint mitigation of laser phase noise, nonlinearity, and FO, we consider PM-16-QAM and PM-QPSK systems. The two systems operate at 50 Gbaud
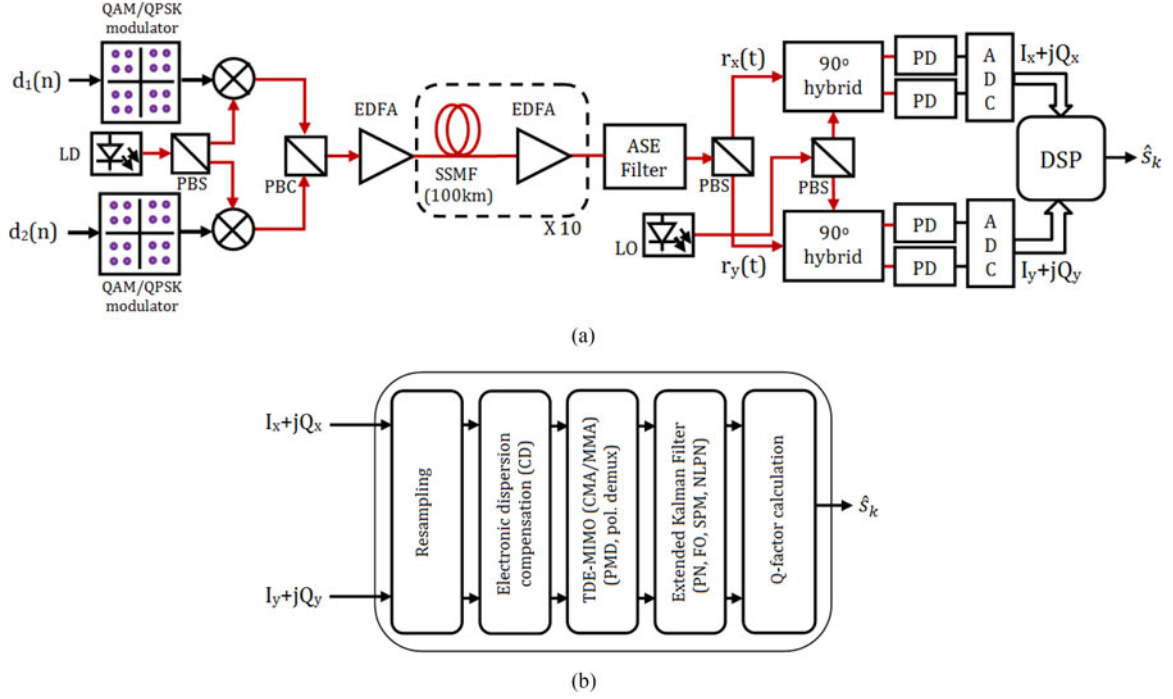
Fig. 1. (a) Simulation model for 50 Gbaud PM-16-QAM/PM-QPSK transmission system. (b) DSP algorithms used at the receiver end. LD: laser diode, PBS: polarization beam splitter, PBC: polarization beam combiner, EDFA: erbium doped fiber amplifier, SSMF: standard single mode fiber, ASE: amplified spontaneous emission noise, LO: local oscillator, PD: photodetector, ADC: analog-to-digital converter, DSP: digital signal processing. Red line: optical fiber, black line: electric wire.

with an overall data rate of 400 and 200 Gbps, respectively. Fig. 1(a) shows a schematic of our transmission model for the 50 Gbaud PM-16-QAM/PM-QPSK system. At the transmitter, the symbols $d_1(n)$ and $d_2(n)$ are QAM or QPSK modulated onto the x and y polarizations of the laser. The baseband modulated signals for 16-QAM and QPSK are given by

$$16\text{-QAM}: \quad s_{x,y}(t) = \sqrt{P_{in}} \cos\left(\frac{u_I(t)\pi}{2V_\pi}\right) \exp\left(\frac{j u_P(t)\pi}{V_\pi}\right)$$

$$u_I(t) = -V_\pi + \frac{2V_\pi}{\pi} \sum_k \left(\arcsin\left(\frac{\sqrt{i_k^2 + q_k^2}}{\sqrt{2}}\right) . p(t - kT_s)\right)$$

$$u_P(t) = \frac{V_\pi}{\pi} \sum_k (\arg[i_k, q_k].p(t - kT_s)) \tag{2}$$

$$\text{QPSK}: \quad s_{x,y}(t) = \sqrt{P_{in}} \exp\left(\frac{j u_1(t)\pi}{V_\pi}\right) \exp\left(\frac{j u_2(t)\pi}{V_\pi}\right)$$

$$u_n(t) = \frac{V_\pi}{2^{n-1}} \sum_k [b_{n_k}.p(t - kT_s)] \tag{3}$$

where i_k and q_k represent the normalized coordinates of kth 16-QAM symbol; b_{n_k} represents the nth bit of a QPSK symbol in the kth symbol interval [21]. The pulse shaping function $p(t - kT_s)$ = 1 for the NRZ case used in the system. The symbols are then combined using a polarization beam combiner (PBC), amplified using power-controlled erbium doped fiber amplifier (EDFA) and transmitted through the channel consisting 10-spans (100 km each) of standard single mode fiber

(SSMF) and in-line amplifiers. The amplifiers used within a span are gain-controlled and assumed to fully compensate the span losses. The received signal vector can be represented as $\mathbf{r_r}(t) = [r_x(t), r_y(t)]^T$ and is given by

$$\mathbf{r_r}(t) = (\mathbf{r_t}(t) \star \mathbf{h_l}(t))h_{nl}(t) + \mathbf{n}(t) \tag{4}$$

$\mathbf{r_t}(t)$ is the transmitted signal given by $\mathbf{r_t}(t) = \mathbf{s}(t)\exp(j\theta(t))$, where $\mathbf{s}(t) = [s_x(t), s_y(t)]^T$ and $\theta(t)$ is the PN of the source laser. $\mathbf{n}(t) = [n_x(t), n_y(t)]^T$ is the noise vector. $\mathbf{h_l}(t)$ and $h_{nl}(t)$ are the linear and nonlinear impulse responses of the channel respectively and are given by

$$\mathbf{h_l}(t) = \mathcal{F}^{-1}\left\{ \begin{pmatrix} \cos\xi & -\sin\xi \\ \sin\xi & \cos\xi \end{pmatrix} \begin{pmatrix} e^{j\omega\tau/2} & 0 \\ 0 & e^{-j\omega\tau/2} \end{pmatrix} \begin{pmatrix} \cos\xi & \sin\xi \\ -\sin\xi & \cos\xi \end{pmatrix} e^{-j\omega^2 \frac{\beta_2}{2} L_{(fiber)}} \right\} \tag{5}$$

$$h_{nl} = \exp\left[j(\theta^{NL}(t) + \Phi(t))\right] \tag{6}$$

where, ξ is the angle between the reference polarization and principal state of polarization (PSP) of the fiber; τ is the differential group delay between the PSPs; β_2 is dispersion coefficient; and $\theta^{NL}(t)$ is the phase shift due to SPM and $\Phi(t)$ is the NLPN due to interaction of SPM with ASE noise [22].

At the receiver, $\mathbf{r_r}(t)$ is filtered using a second-order Gaussian bandpass filter to reduce the out-of-band ASE noise. The two polarizations of the received signal, $r_x(t)$ and $r_y(t)$ are separated using a polarization beam splitter (PBS) and demodulated using a polarization diverse coherent receiver with a local oscillator (LO). The LO laser is considered free of phase noise, with a fixed frequency offset (FO). FO is the fixed frequency difference between transmitter laser and LO. The $r_x(t)$ and $r_y(t)$ signals are downconverted using photodetectors and sampled by the ADCs. The in-phase and quadrature components of each polarization thus extracted, are combined to form complex discrete signal samples r_x and r_y, where $r_x = I_x + jQ_x$ and $r_y = I_y + jQ_y$. r_x and r_y are then processed using a DSP module expanded in Fig. 1(b).

The DSP module consists of successive application of the following four algorithms: (a) Resampling to resample the incoming ADC samples at twice the symbol rate, (b) Electronic dispersion compensation (EDC) using overlap FDE method to mitigate the acclumulated chromatic dispersion (CD) [23], (c) Adaptive TDE-MIMO algorithm to compensate polarization mode dispersion (PMD) and polarization crosstalk in the linearly equalized samples and separate out the two polarizations [5]. It is adapted by constant modulus algorithm (CMA) for QPSK and multi-modulus algorithm (MMA) for 16-QAM with optimized number of taps. The data of x and y polarizations are then sampled to one sample/s and fed to the EKF for further processing. (d) EKF to mitigate laser PN, FO and nonlinearity and this process is described in detail in the next section. We have used EKF for each polarization separately. However, the two polarizations can be jointly considered along with other impairments [15].

3. Extended Kalman Filtering

After compensation of the linear impairments CD and PMD, (4) is reduced to the form $\mathbf{r_k} = \mathbf{s_k}\exp(j\Psi_k) + \mathbf{n_k}$, where $\mathbf{r_k} = [r_{k_x} r_{k_y}]^T$. For simplicity, we drop the vector notation and represent r_{k_x} and r_{k_y} individually by r_k as

$$r_k = s_k\exp(j\Psi_k) + n_k \tag{7}$$

where k denotes the kth sample over the observed 16-QAM/QPSK symbol. s_k are the samples of modulated signal, given by $s_k = \sqrt{P_{in}}d_k$, where P_{in} is the input launch power and d_k are the mapped data symbols represented by $[\pm 1/3\pm 1/3j, \pm 1/3\pm 1j, \pm 1\pm 1/3j, \pm 1\pm 1j]$ for 16-QAM and $[\pm 1, \pm 1j]$ for QPSK. $\Psi_k = \omega_k T + \theta_k + \theta_k^{NL} + \Phi_k$ is the uncompensated phase due to frequency offset, inherent phase noise of the laser diode at the transmitter and fiber nonlinearity; where, ω_k is the fixed frequency offset at LO, T is the symbol duration, θ_k is the laser PN, θ_k^{NL} is the average fixed SPM phase and Φ_k is the NLPN. n_k is the complex ASE noise sample modeled as zero mean AWGN process.
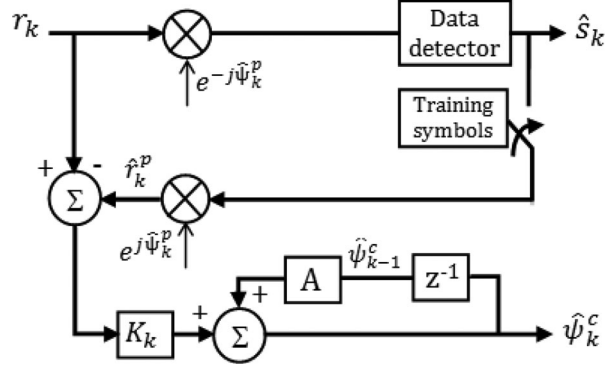
Fig. 2. Schematic diagram of EKF for FO, PN, and nonlinearity estimation.

We model the laser phase noise at the transmitter as a discrete Weiner process: $\theta_k = \theta_{k-1} + \delta\theta_k$. $\delta\theta_k$ is a zero-mean Gaussian random variable with a variance of $\sigma_\theta^2 = 2\pi\delta\nu/R$, where $\delta\nu$ denotes full-width half-maximum (FWHM) linewidth of the laser and R is the data rate of the transmission system. The fixed aevarage SPM phase shift for N spans is given by $\theta_k^{NL} = N\gamma L_{\text{eff}}[P_{\text{in}} + (N + 1)\sigma_n^2]$ $\approx N\gamma L_{\text{eff}}P_{\text{in}}$, where γ is the nonlinear coefficient, L_{eff} is the effective length of SSMF within one span, N is the total no. of spans and σ_n^2 is the variance of ASE noise [10]. Φ_k is the resultant phase due to NLPN with variance $\sigma_\Phi^2 = (4/3)N^3(\gamma L_{\text{eff}})^2 P_{\text{in}}\sigma_n^2$.

Two-state EKF model for frequency and phase estimation:

The complex discrete samples, r_k of each polarization are processed using a two-state EKF for the estimation and compensation of FO, PN and nonlinearity. The schematic diagram of EKF is shown in Fig. 2. We take $[\Psi_k, \omega_k]^T$ as the two-component state vector. The state model is given by

$$\begin{pmatrix} \Psi_{k+1} \\ \omega_{k+1} \end{pmatrix} = \begin{pmatrix} 1 & 1 \\ 0 & 1 \end{pmatrix} \begin{pmatrix} \Psi_k \\ \omega_k \end{pmatrix} + \begin{pmatrix} w_{1k} \\ w_{2k} \end{pmatrix} \tag{8}$$

where Ψ_k is the uncompensated phase due to offsets and phase noises at the kth sample, ω_k is the LO frequency offset, and w_{1k} and w_{2k} are the process noises assumed to have Gaussian probability density function (PDF). r_k is taken as measurement variable, represented as $r_k = s_k \exp(j\Psi_k) + n_k$, where n_k is the measurement noise modelled as AWGN process. The estimates of Ψ_k and ω_k are obtained using the following recursive EKF equations:

Prediction stage :
$$\hat{\Psi}_k^p = \hat{\Psi}_{k-1}^c + \hat{\omega}_{k-1}^c$$
$$\hat{\omega}_k^p = \hat{\omega}_{k-1}^c$$
$$P_k^p = A P_{k-1}^c A^T + Q$$
$$\hat{r}_k^p = \hat{s}_k \exp(j\hat{\Psi}_k^p) \tag{9}$$

Correction stage :
$$H_k = \begin{pmatrix} -\Im(\hat{r}_k^p) & \Re(\hat{r}_k^p) \\ 0 & 0 \end{pmatrix}$$
$$K_k = P_k^p (H_k^*)^T (H_k P_k^p (H_k^*)^T + R)^{-1}$$
$$P_k^c = P_k^p - K_k H_k P_k^p$$
$$\begin{pmatrix} \hat{\Psi}_k^c \\ \hat{\omega}_k^c \end{pmatrix} = A \begin{pmatrix} \hat{\Psi}_{k-1}^c \\ \hat{\omega}_{k-1}^c \end{pmatrix} + K_k \begin{pmatrix} \Re(r_k - \hat{r}_k^p) \\ \Im(r_k - \hat{r}_k^p) \end{pmatrix} \tag{10}$$
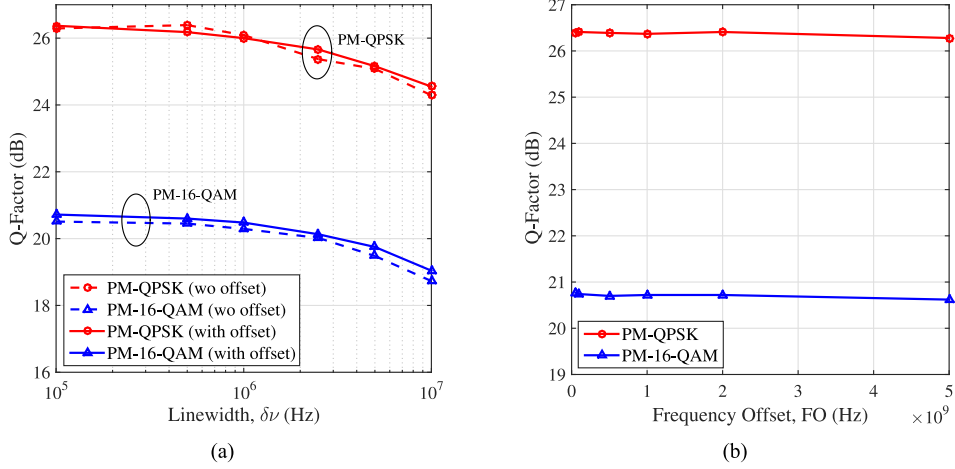
Fig. 3. Performance for b2b propagation. (a) Q-factor vs. linewidth $\delta\nu$ with and without FO of 1 GHz. (b) Q-factor vs. frequency offset, FO at $\delta\nu = 100$ kHz.

where A is the state transition matrix given by $\begin{pmatrix} 1 & 1 \\ 0 & 1 \end{pmatrix}$, K_k is the Kalman gain, and Q and R are the covariance matrices of process and measurement noise, respectively. The performance of EKF depends on Q and R. As Q increases, the filter bandwidth increases giving rise to faster transient response. But with an increase in Q, the error covariance P also increases indicating a rise in uncertainty [24]. The same effect is also observed by decreasing R. In our simulations, Q and R are calculated as $Q = Q_o I_2$ and $R = R_o I_2$ where, I_2 is a 2x2 identity matrix. Q_o and R_o are initiated with σ_θ^2 and $N\sigma_n^2$ respectively and tuned further to achieve a better tradeoff between fast acquisition and small phase tracking error. The estimation is initiated with $\hat{\Psi}_0^c$ and $\hat{\omega}_0^c$ set as 0 and P_0^c taken to be I_2 [25]. The discrete symbols r_k are first derotated by $\hat{\Psi}_k^p$ to produce soft decisions on the QAM/QPSK symbols $\hat{s}_k$ which are used in estimating the state in the next iteration as shown in Fig. 2. The estimates $\hat{\Psi}_k^c$ are used to derotate $r_k \Rightarrow r_k \exp(-j\hat{\Psi}_k^c)$, thereby giving the correct estimates of s_k.

4. Results and Discussion

In this section, we discuss the performance of EKF for mitigating PN, FO and nonlinearity in 400 Gbps PM-16-QAM and 200 Gbps PM-QPSK systems. The system model used in simulation is shown in Fig. 1(a). We evaluate the performance in terms of Q-factor for both back-to-back (b2b) and fiber transmission. Q-factor is calculated on the basis of error vector magnitude (EVM) given in [26], [27], with the following simplified equations:

$$\text{BER}_{(QPSK)} = \frac{1}{2} erfc\left(\frac{1}{\sqrt{2}EVM}\right); \quad \text{BER}_{(QAM)} = \frac{3}{8} erfc\sqrt{\frac{\sqrt{2}}{10EVM^2}} \tag{11}$$

$$Q(dB) = 20\log_{10}(\sqrt{2}erfc^{-1}(2\text{BER})) \tag{12}$$

For b2b transmission, the channel is bypassed in the simulation, while for fiber transmission, a total of 10 spans each of 100 km leading to a total link length of 1000 km is used. Further, for b2b transmission, the filter is operated in decision-directed mode without using any training symbols. However, for span transmission the filter is operated in the data-aided mode for the first 5 time samples and then switched to the decision-directed mode. In both the cases, a total number of 2^{14} symbols are transmitted. We used VPI transmission maker 9.5 to simulate the system shown in Fig. 1(a) and processed the data using MATLAB.
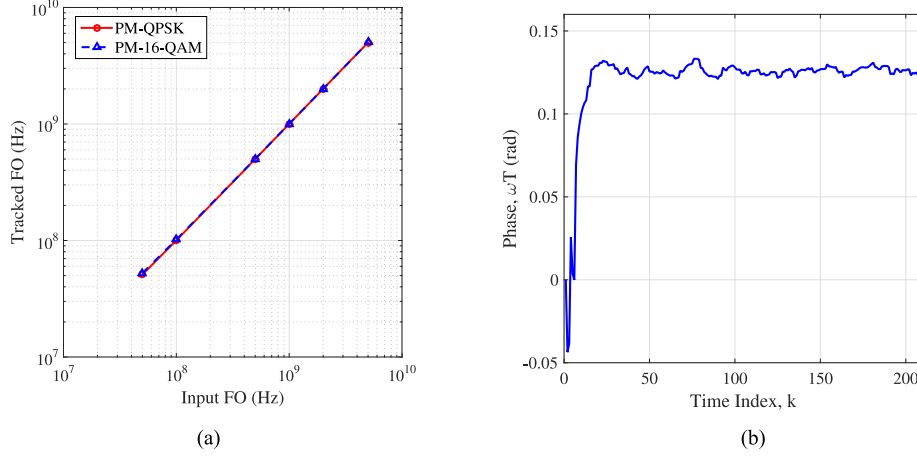
Fig. 4. FO estimation. (a) Tracked FO vs. input FO. (b) Tracked phase offset corresponding to FO of 1 GHz.

4.1. B2B Transmission

For b2b propagation, we set the launch power P_{in} to 0 dBm. Since fiber is not included in this case, the EKF tracks and compensates laser PN and FO only. Fig. 3(a) shows the graph of Q-factor as a function of laser linewidth, $\delta\nu$ for PM-16-QAM and PM-QPSK for two cases: without considering LO-frequency offset, i.e., FO = 0 GHz, and with FO of 1 GHz. We observe that the Q-factors, with FO taken into account, coincide with the case without FO for both modulated formats. Moreover, a Q-factor of ≈19 dB and 24.5 dB are achieved for PM-16-QAM and PM-QPSK respectively even at a linewidth as high as 10 MHz.

Fig. 3(b) shows Q-factor as a function of FO while linewidth of the laser is kept fixed at 100 kHz. We observe that the Q-factor remains nearly constant for all the values of FO from 50 MHz to 5 GHz. Thus, we conclude that EKF can eliminate offsets as large as 5 GHz. This is further justified by Fig. 4(a) where the FO tracked by EKF is plotted against the FO applied to the system. We see that estimated FO coincides with the applied FO for both PM-16-QAM and PM-QPSK. The tracked phase offset corresponding to FO of 1 GHz is shown in Fig. 4(b). The tracked FO trajectory shows that the filter converges within <20 symbols.

4.2. Span Transmission

We simulate the PM-16-QAM/QPSK modulated system transmitted over 10 spans (10 × 100 km) as shown in Fig. 1(a). Each span of the channel consists of SSMF simulated using the split-step fourier method (SSFM) for attenuation, α = 0.2 dB/km; dispersion, D = 17 ps/nm-km; dispersion slope, S = 0.08e^3 s/m^3; nonlinear coefficient, γ = 1.3/W/km and PMD, D_P = 0.01 ps/$\sqrt{km}$. The SSMF within a span is followed by an EDFA with gain, G = 20 dB to compensate for span losses. The EDFA noise figure is taken to be 3.5 dB. At the receiver, a second order Gaussian band pass filter is used to reduce out-of-band ASE noise. After coherent detection, the signal is processed with DSP module. Electronic dispersion compensation using overlap FDE method is used to compensate for CD and TDE-MIMO (using adaptive CMA/MMA) is used for mitigating PMD. For the mitigation of FO, PN and nonlinearity, the EKF algorithm is used as explained in Section III. In this section we also compare the Q-factor performance of EKF with that of CPANE assuming FO = 0 for the latter.

Fig. 5(a) shows the plot of Q-factor vs. input launch power P_{in} for PM-16-QAM and PM-QPSK under three scenarios: a) without FO-EKF, where FO = 0 GHz and EKF is used to mitigate PN and nonlinearity; b) with FO-EKF where EKF tracks PN and nonlinearity along with FO of 1 GHz; c) without FO-CPANE, where FO = 0 GHz and CPANE is used to mitigate PN and nonlinearity. Laser linewidth is fixed at 100 kHz for PM-16-QAM and 1 MHz for PM-QPSK systems.
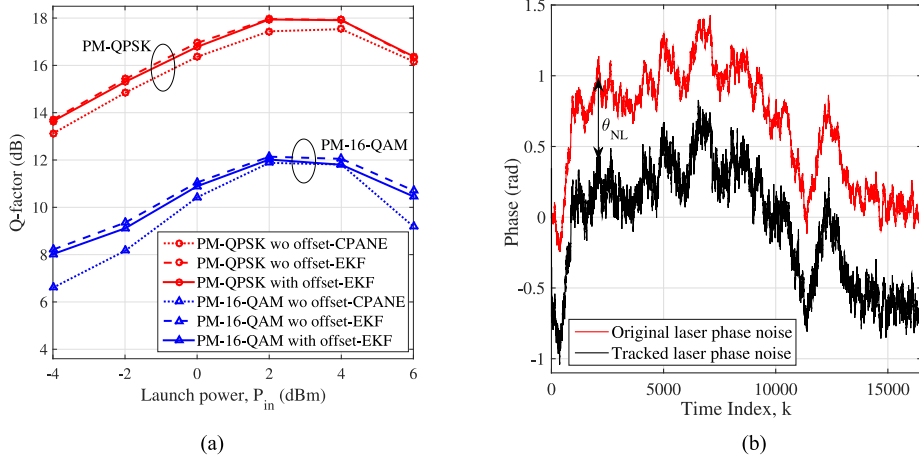
Fig. 5. Performance for span transmission. (a) Q-factor vs. launch power. N = 10 spans, FO = 1 GHz, $\delta\nu_{(QPSK)}$ = 1 MHz, and $\delta\nu_{(QAM)}$ = 100 kHz. (b) Tracked phase noise at EKF output. P_{in} = 2 dBm, N = 10 spans, $\delta\nu$ = 1 MHz, and FO = 0 GHz.
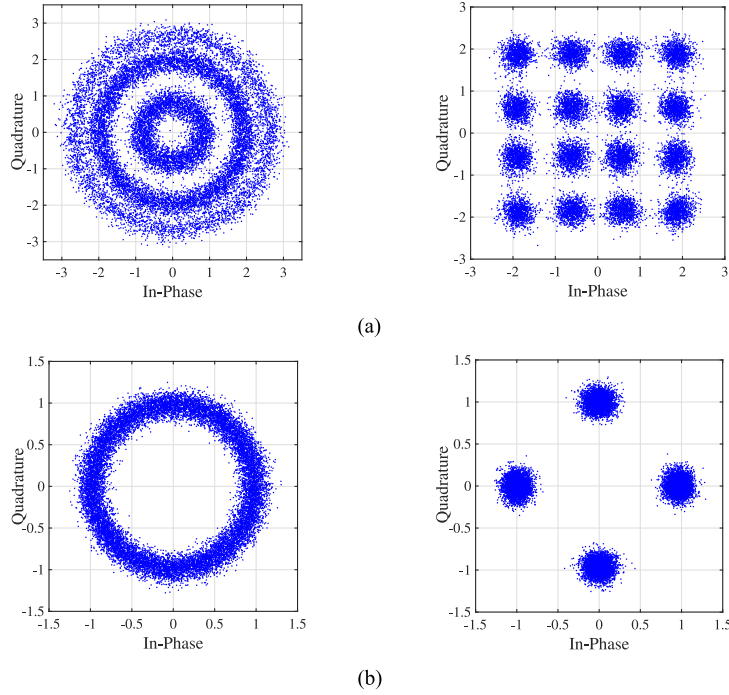

Fig. 6. Constellation diagrams before and after EKF at P_{in} = 2 dBm, FO = 1 GHz and N = 10 spans. (a) PM-16-QAM system at $\delta\nu$ = 100 kHz. (b) PM-QPSK system at $\delta\nu$ = 1 MHz.

We see that Q-factor performance for cases a) and b) coincide with each other for both systems and a maximum Q-factor of ≈12 and 18 dB are achieved for PM-16-QAM and PM-QPSK respectively for P_{in} = 2 dBm. This shows that EKF is capable of compensating PN and nonlinearity along with high FO (of 1 GHz) without severe performance degradation. Comparing cases a) and b) with case c), we find that EKF performs better than CPANE by ≈0.3 dB for PM-16-QAM and ≈0.5 dB for PM-QPSK at 2 dBm. Further, for PM-16-QAM, the performance difference rises to ≈1.5 dB at 6 dBm. While due to scalar EKF, CPANE has reduced complexity as compared to two-state EKF in

this paper, but in the presence of FO the former does not converge. To compensate FO, a separate algorithm should be used or CPANE should be reformulated by adding FO as another state variable. In both the cases, the complexity of the overall parameter estimation rises which cannot be avoided. The advantage of using a single EKF is not only in terms of Q-factor but also the fact that EKF eliminates PN, nonlinearity and a high FO of 1 GHz simultaneously and does not require separate algorithms.

Fig. 5(b) shows the original and tracked PN trajectories at P_{in} = 2 dBm, N = 10 spans, and $\delta\nu$ = 1 MHz. We observe that the tracked PN is similar to the original PN. The phase difference between the two trajectories corresponds to the fixed average phase shift due to SPM, i.e., θ^{NL} as explained in Section III.

Fig. 6(a) and (b) shows the constellation diagrams for PM-16-QAM and PM-QPSK, respectively, before and after using EKF. They are captured at P_{in} = 2 dBm, after transmission over 10 spans. $\delta\nu$ is set at 100 kHz for PM-16-QAM and 1 MHz for PM-QPSK while maintaining FO of 1 GHz. While the presence of nonlinearity gives a fixed phase shift to the constellation points along with the helical-shaped distribution due to NLPN, high PN and FO in the system also tend to rotate the constellation diagram exhibiting the arcs about the ideal points. Due to the combined effect of these impairments, the constellation diagram tends to close [28], [29]. We observe in Fig. 6(a) and (b) that for both the cases, constellation diagram is initially closed due to the presence of PN, FO and nonlinearity in the system. After applying EKF, the constellation points return to their original positions indicating the elimination of impairments. The uniform spread around the points is attributed to ASE noise present in the system.

5. Conclusion

In this paper, we demonstrated the use of the extended Kalman filter to track and mitigate laser phase noise, frequency offset and nonlinearity for 50 Gbaud coherent PM-16-QAM (400 Gbps) and PM-QPSK (200 Gbps) systems. Simulations are carried out for back-to-back transmission and channel transmission over 10 × 100 km with frequency offset as high as 1 GHz. For back-to-back transmission, we obtained a Q-factor of 19 dB for PM-16-QAM and 24.5 dB for PM-QPSK at high linewidth of 10 MHz. For span transmission, maximum Q-factor of 12 dB is achieved for PM-16-QAM at a linewidth of 100 kHz and 18 dB is obtained for PM-QPSK at 1 MHz linewidth. We also provide phase trajectories corresponding to laser phase noise and frequency offsets which shows that EKF can suppress laser phase noise up to 10 MHz and frequency offset up to 5 GHz. Constellations diagrams obtained after EKF seem to be consistent with the original signal constellations proving that EKF can jointly mitigate multiple impairments thereby eliminating the requirement of separate algorithms. Thus, EKF can be an interesting and optimized choice for joint mitigation of laser PN, FO, and nonlinearities.

Acknowledgment

References

[1] X. Zhou and L. E. Nelson, "400G WDM transmission on the 50 GHz grid for future optical networks," *J. Lightw. Technol.*, vol. 30, no. 24, pp. 3779–3792, Dec. 2012.

[2] G. Raybon *et al.*, "Single-carrier 400G interface and 10-channel WDM transmission over 4800 km using all-ETDM 107-Gbaud PDM-QPSK," in *Proc. Opt. Fiber Commun. Conf./Nat. Fiber Opt. Eng. Conf.*, 2013, Paper PDP5A.5.

[3] A. Rezania and J. C. Cartledge, "Transmission performance of 448 Gb/s Single-Carrier and 1.2 Tb/s Three-Carrier superchannel using dual-polarization 16-QAM with fixed LUT based MAP detection," *J. Lightw. Technol.*, vol. 33, no. 23, pp. 4738–4745, Dec. 2015.

[4] A. Leven, N. Kaneda, U.-V. Koc, and Y.-K. Chen, "Frequency estimation in intradyne reception," *IEEE Photon. Technol. Lett.*, vol. 6, no. 19, pp. 366–368, Mar. 2007.

[5] M. Kuschnerov *et al.*, "DSP for coherent single-carrier receivers," *J. Lightw. Technol.*, vol. 27, no. 16, pp. 3614–3622, Aug. 2009.

[6] M. G. Taylor, "Phase estimation methods for optical coherent detection using digital signal processing," *J. Lightw. Technol.*, vol. 27, no. 7, pp. 901–914, Apr. 2009.

[7] E. Ip, "Nonlinear compensation using backpropagation for polarization-multiplexed transmission," *J. Lightw. Technol.*, vol. 28, no. 6, pp. 939–951, Mar. 2010.

[8] D. S. Millar *et al.*, ''Mitigation of fiber nonlinearity using a digital coherent receiver," *IEEE J. Sel. Topics Quantum Electron.*, vol. 16, no. 5, pp. 1217–1226, Sep./Oct. 2010.

[9] S. Kumar, "Analysis of nonlinear phase noise in coherent fiber-optic systems based on phase shift keying," *J. Lightw. Technol.*, vol. 27, no. 21, pp. 4722–4733, Nov. 2009.

[10] K.-P. Ho and J. M. Kahn, "Electronic compensation technique to mitigate nonlinear phase noise," *J. Lightw. Technol.*, vol. 22, no. 3, pp. 779–783, Mar. 2004.

[11] E. Ip and J. M. Kahn, "Feedforward carrier recovery for coherent optical communications," *J. Lightw. Technol.*, vol. 25, no. 9, pp. 2675–2692, Sep. 2007.

[12] S. S. Haykin, Ed. *Kalman Filtering and Neural Networks*. New York, NY, USA: Wiley, 2001.

[13] M. S. Grewal and A. P. Andrews, *Kalman filtering: Theory and practice Using MATLAB*, 2nd ed. New York, NY, USA: Wiley, 2001.

[14] L. Barletta, M. Magarini, and A. Spalvieri, "Bridging the gap between Kalman filter and Wiener filter in carrier phase tracking," *IEEE Photon. Technol. Lett.*, vol. 25, no. 11, pp. 1035–1038, Jun. 2013.

[15] B. Szafraniec, T. S. Marshall, and B. Nebendahl, "Performance monitoring and measurement techniques for coherent optical systems," *J. Lightw. Technol.*, vol. 31, no. 4, pp. 648–663, Feb. 2013.

[16] S. Zhang, P. Y. Kam, C. Yu, and J. Chen, "Frequency offset estimation using a Kalman filter in coherent optical phase-shift keying systems," in *Proc. Conf. Lasers and Electro-Optics*, 2010, Paper CThDD4.

[17] A. Jain and P. Krishnamurthy, "Phase noise tracking and compensation in coherent optical systems using Kalman filter," *IEEE Commun. Lett.*, vol. 20, no. 6, pp. 1072–1075, Jun. 2016.

[18] A. Jain, P. K. Krishnamurthy, P. Landais, and P. M. Anandarajah, "Extended kalman filter for estimation of phase noises and frequency offset in 400G PM-16-QAM systems," in *Proc. Int. Conf. Fibre Opt. Photon.*, 2016, Paper Tu3A-3.

[19] L. Pakala and B. Schmauss, "Extended Kalman filtering for joint mitigation of phase and amplitude noise in coherent QAM systems," *Opt. Exp.*, vol. 24, no. 6, pp. 6391–6401, 2016.

[20] S. Hoffmann *et al.*, "Frequency and phase estimation for coherent QPSK transmission with unlocked DFB lasers," *IEEE Photon. Technol. Lett.*, vol. 20, no. 18, pp. 1569–1571, Sep. 2008.

[21] M. Seimetz, *High-Order Modulation for Optical Fiber Transmission*. Berlin, Germany: Springer, vol. 143, 2009.

[22] A. Mecozzi, "Probability density functions of the nonlinear phase noise," *Opt. Lett.*, vol. 29, no. 7, pp. 673–675, 2004.

[23] R. Kudo, T. Kobayashi, K. Ishihara, Y. Takatori, A. Sano, and Y. Miyamoto, "Coherent optical single carrier transmission using overlap frequency domain equalization for long-haul optical systems," *J. Lightw. Technol.*, vol. 27, no. 16, pp. 3721–3728, Aug. 2009.

[24] J. V. Candy, *Model-Based Signal Processing*, vol. 36. Hoboken, NJ, USA: Wiley, 2005.

[25] W.-T. Lin and D.-C. Chang, "The extended Kalman filtering algorithm for carrier synchronization and the implementation," in *Proc. IEEE Int. Symp. Circuits Syst.*, 2006, 4 pp.

[26] F. Zhang *et al.*, "Experimental comparison of different BER estimation methods for coherent optical QPSK transmission systems," *IEEE Photon. Technol. Lett.*, vol. 23, no. 18, pp. 1343–1345, Sep. 2011.

[27] R. Schmogrow *et al.*, "Error vector magnitude as a performance measure for advanced modulation formats," *IEEE Photon. Technol. Lett.*, vol. 24, no. 1, pp. 61–63, Jan. 2012.

[28] E. Ip, A. P. T. Lau, D. J. F. Barros, and J. M. Kahn, "Coherent detection in optical fiber systems," *Opt. Exp.*, vol. 16, no. 2, pp. 753–791, 2008.

[29] J. Hong Ke, K. P. Zhong, Y. Gao, J. C. Cartledge, A. S. Karar, and M. A. Rezania, "Linewidth-tolerant and low-complexity two-stage carrier phase estimation for dual-polarization 16-QAM coherent optical fiber communications," *J. Lightw. Technol.*, vol. 30, no. 24, pp. 3987–3992, Dec. 2012.